Delivery of melarsoprol using folate-targeted PEGylated cyclodextrin-based nanoparticles for hepatocellular carcinoma

Ya-Nan Li [a], Xiaoju Shi [b], Dandan Sun [c], Shulan Han [c], Yifang Zou [c], Lingzhi Wang [c], Leilei Yang [c], Yutong Li [c], Ying Shi [d] *, Jianfeng Guo [c] *, and Caitriona M O'Driscoll [e]

[a]Department of Pediatrics, The First Hospital of Jilin University, Changchun 130021, China

[b]Department of Hepatobiliary and Pancreatic Surgery, The First Hospital of Jilin University, Changchun 130021, China

[c]School of Pharmaceutical Sciences, Jilin University, Changchun 130021, China

[d]Department of Hepatology, The First Hospital of Jilin University, Changchun 130021, China

[e]Pharmacodelivery Group, School of Pharmacy, University College Cork, Cork T12 YN60, Ireland

* **Corresponding authors**: jguo@jlu.edu.cn (J Guo) and shiy707@jlu.edu.cn (Y Shi)

Abstract

Hepatocellular carcinoma (HCC) is the most common type of primary liver cancer, and has become one of the most lethal malignancies in the world. Although chemotherapy remains a cornerstone of cancer therapy, the number of chemotherapeutic drugs approved for HCC is low, and emerging therapeutics are needed. Melarsoprol (MEL) is an arsenic-containing drug, and has been applied in the treatment of human African trypanosomiasis at the late stage. In this study, the potential of MEL for HCC therapy was investigated for the first time using *in vitro* and *in vivo* experimental approaches. A folate-targeted polyethylene glycol-modified amphiphilic cyclodextrin nanoparticle was developed for safe, efficient and specific delivery of MEL. Consequently, the targeted nanoformulation achieved cell-specific uptake, cytotoxicity, apoptosis and migration inhibition in HCC cells. Furthermore, the targeted nanoformulation significantly prolonged the survival of mice with orthotopic tumor, without causing toxic signs. This study indicates the potential of the targeted nanoformulation as an emerging chemotherapy option for treating HCC.

Keywords: liver cancer, drug delivery, nanoparticle, arsenicals, chemotherapy.

1. Introduction

Hepatocellular carcinoma (HCC) is the most common primary liver cancer, with estimated new cases and deaths over 680,000 and 620,000 respectively in 2020 worldwide (Sung et al., 2021). Since the majority of HCC patients are diagnosed at an advanced stage, they can only be treated using systemic therapies, including chemotherapy, targeted therapy (e.g., multi-kinase inhibitors), and immunotherapy (e.g., immune checkpoint inhibitors) (Galle et al., 2021). However, the efficacy of these therapies is low, and the overall survival of patients is only increased by 3 to 9 months (Llovet et al., 2018). Chemotherapy is among the most effective strategies in many types of cancer, but the number of chemotherapeutic drugs approved for HCC is low. Therefore, therapeutic breakthroughs in chemotherapy are needed.

Melarsoprol (MEL) is an arsenic (As)-containing drug with a structure containing melarsen oxide and dimercaptopropanol (Fig. 1), and has been exclusively applied for late-stage human African trypanosomiasis (sleeping sickness) (Fairlamb and Horn, 2018). MEL is characterized as a highly lipophilic drug with a logP of 2.53 and a water solubility of 6 mg/L at 25 ºC (Gibaud et al., 2005). The lipophilic nature allows MEL to cross the blood brain barrier (BBB) for killing trypanosome parasites residing in the cerebrospinal fluid (CSF) (Fairlamb and Horn, 2018). However, the feasibility of MEL in the treatment of sleeping sickness is dramatically limited by severe toxicities, such as tissue necrosis around the injection location, neuropathy, and gastrointestinal upset (Kennedy, 2006). The β-cyclodextrin (CD; a cyclic oligosaccharide with seven macrocyclic rings of glucose units) has been widely applied to improve the solubility and bioavailability of hydrophobic molecules. Recently, Kennedy and colleagues have developed two CD derivatives that were termed as randomly methylated CD (RAME-CD) and hydroxypropyl CD (HP-CD) (Gibaud et al., 2005). MEL could be complexed

with two CD derivatives at molar ratio of 1:1, forming RAME-CD.MEL and HP-CD.MEL microcomplexes, respectively (Gibaud et al., 2005). Following systemic administration, these microcomplexes were mainly delivered into the brain, in which they exerted therapeutic function against the trypanosome infection in mice (Ben Zirar et al., 2008) (Rodgers et al., 2011).

Since As is perceived as a promising agent for cancer therapy, it is hypothesized that MEL may achieve anti-HCC efficacy. Recently, a folate (FA)-targeted polyethylene glycol (PEG)-modified amphiphilic CD nanoparticle (NP) has been developed in our laboratories for *in vitro* and *in vivo* delivery of chemotherapeutic drugs (Zou et al., 2021) (Sun et al., 2022). Since folate receptor (FR) is highly expressed on the membrane surface of liver cancer cells (Koirala et al., 2019), the FA-targeted PEGylated CD NP was used in this study for delivery of MEL to HCC. Consequently, the targeted nanoformulation (namely CD.MEL.PEG-FA) facilitated HCC-specific delivery of MEL *via* FR, achieving significantly higher cellular uptake, cytotoxicity, apoptotic cell death and cell migration inhibition in comparison with the non-targeted counterpart (CD.MEL.PEG). Following intravenous (i.v.) administration in orthotopic HCC mice, CD.MEL.PEG-FA significantly retarded tumor development and promoted animal survival, without causing obvious toxic effects.

2. Materials and Methods

2.1. Materials

MEL ($C_{12}H_{15}AsN_6OS_2$, M_W = 398.341 g/mol; Fig. 1) was purchased from Toronto Research Chemicals Inc. (Toronto, Canada). 1,2-distearoyl-sn-glycero-3-phosphoethanolamine-N-[methoxy(polyethylene glycol)-2000] (DSPE-mPEG$_{2000}$) and 1,2-distearoyl-sn-glycero-3-phosphoethanolamine-N-[folate(polyethylene glycol)-

2000] (DSPE-PEG_{2000}-Folate) were purchased from Xi'an Biological Technology Co., Ltd. (Xi'an, China). The other materials were obtained from Sigma-Aldrich unless mentioned otherwise.

2.2. Nanoformulation preparation

The amphiphilic CD was produced as previously described (O'Mahony et al., 2012). As shown in Fig. 1, in order to prepare the targeted nanoformulation, 5 mg of CD and 1 mg of MEL were dissolved in 50 mL of methanol (MeOH) and dried to form a thin film using a rotary evaporator. This content was rehydrated within 3 mL of ultrapure water and sonicated at 37 ºC for 1-2 h, in order to achieve the CD.MEL nanocomplex. As previously described (Zou et al., 2021), 3.5 mg of DSPE-$mPEG_{2000}$ (DSPE-PEG) and 1 mg of DSPE-PEG_{2000}-FA (DSPE-PEG-FA) (molar ratio ≈ 4:1) were dissolved in 0.5 mL of HEPES buffer (20 mmol/L, pH = 7.4) and incubated at 60 ºC for 30 min to obtain a solution. The solution was added into the CD.MEL nanocomplex and incubated at 60 ºC with shaking for 1-1.5 h, in order to achieve the targeted nanoformulation (CD.MEL.PEG-FA) (~ 5 mol% of FA in the outer surface per NP in theory). The non-targeted nanoformulation (CD.MEL.PEG) was prepared as described above without the incorporation of DSPE-PEG-FA. The nanoformulations containing rhodamine or DiR (0.05%, w/w) were prepared as described above by dissolving CD, MEL and rhodamine (or DiR) in MeOH.

2.3. Physicochemical characterization of nanoformulation

The encapsulation efficiency (EE%) and loading capacity (LC%) of MEL were measured using high performance liquid chromatography (HPLC; Shimadzu, Japan) (C18 column; UV at 285 nm; mobile phase = acetonitrile and water, v:v = 70:30) and calculated using the equations as follows: EE% = (weight of loaded MEL/weight of feed MEL) x 100% and LC% = (weight of loaded MEL/weight of total nanoformulation)

x 100%.

The solution of nanoformulation containing 5 μg MEL was added onto a 400-mesh carbon-filmed copper grid (Agar Scientific) (Guo et al., 2012). The grid was added with 2% (w/w) uranyl acetate, prior to the analysis using transmission electron microscopy (TEM) (JEOL JEM-1230).

The particle size and zeta potential of nanoformulation were assessed using Malvern Nano-ZS as previously described (Luan et al., 2019). In addition, when the nanoformulation was stored at 4 ºC in aqueous solution, the particle size was measured at different time points by Malvern Nano-ZS as previously described (Sun et al., 2022), in order to determine the stability.

The solution of nanoformulation containing 500 μg MEL in a dialysis bag (MWCO = 2 kDa; Solarbio®, China) was incubated in 100 mL of release medium (0.01 M PBS containing 0.5% Tween 80; pH = 5.5 or 7.4) at 37 ºC with stirring. At different time points, 5 mL of supernatant were collected, and 5 mL of fresh release medium were supplemented. The drug concentration within the supernatant was measured using HPLC as described above.

2.4. *In vitro* anti-HCC effects of nanoformulation

Hepa1-6 cells (a mouse HCC cell line with FR (Hu et al., 2017) (Maghsoudinia et al., 2021a) (Maghsoudinia et al., 2021b) (Gong et al., 2021)) were cultured in DMEM with 10% FBS and 1% Penicillin-Streptomycin. Hepa1-6-Luc cells, which can stably express the luciferase, were cultured in DMEM with 10% FBS, 1% Penicillin-Streptomycin, and 1 μg/mL of puromycin (ThermoFisher). All the cells were maintained at 37 ºC with 5% CO_2 and 95% relative humidity.

Hepa1-6 cells (5 x 10^3 cells per well) were seeded in 96-well plates for 24 h. After this, cells were incubated with the nanoformulation at different concentrations of MEL

for 24 h. Subsequently, cells were washed twice with PBS and incubated with 20 μL of MTT reagent (5 mg/mL in PBS) and 180 μL of fresh growth medium at 37 °C for 4 h. The purple precipitate was dissolved by DMSO before the measurement at 570 nm using Microplate Reader.

Hepa1-6 cells (2 x 10^4 cells per well) were seeded in 24-well plates with glass bottoms for 24 h. After this, cells were incubated with PBS or nanoformulations ([c] of MEL = 5 μmol/L MEL; 0.05 % rhodamine, w/w) for 8 h. Subsequently, cells were washed with PBS twice, treated with 4% paraformaldehyde for 20 min, and stained by DAPI (Beyotime Biotech, China). The cellular uptake was assessed using the confocal microscopy (Olympus FV3000) and analyzed using ImageJ to determine the relative fluorescence intensity (%).

Hepa1-6 cells (1 x 10^5 cells per well) were seeded in 6-well plates for 24 h. Subsequently, cells were incubated with PBS or nanoformulations ([c] of MEL = 15 μmol/L) for 24 h, and apoptotic cells (%) were detected using Annexin V-FITC and propidium iodide (PI) (YEASEN Biotech, China) using flow cytometry (BD FACSCalibur).

Hepa1-6 cells (3 x 10^5 cells per well) were seeded in 6-well plates for 24 h. As previously described (Yang et al., 2021), when cells reached the confluence, the cell monolayer was washed with PBS and scraped with a pipette tip. Subsequently, cells were incubated in serum-free growth medium and added with PBS or nanoformulations ([c] of MEL = 15 μmol/L) for 24 h. The cell-free areas before and after treatment of nanoformulations, as a measure of cell migration, were imaged under the light microscope and analyzed using ImageJ.

2.5. *In vivo* toxicity and tumor distribution of nanoformulation

Six to eight week old male C57BL/6 mice were obtained from Beijing Vital River

Laboratory Animal Technology Company. The experiments were approved by the Animal Ethics Committee of Jilin University.

Healthy mice (n = 4) were i.v. injected with PBS or nanoformulations (containing ~ 1 mg/kg of MEL) on Day 1, 5, 9, 12 and 17, and the body weight was regularly recorded. On Day 25, the heart, liver, spleen, lung, kidneys were obtained for the analysis of histopathology, and the serum was collected to evaluate the hepatic/renal functions, as previously described (Guo et al., 2020).

As previously described (Yu et al., 2020) (Han et al., 2022), mice were anesthetized using 4% chloral hydrate, and 5×10^5 Hepa1-6-Luc cells were injected into the liver lobe to develop orthotopic HCC (Day 0). Animals were intraperitoneally administered 80 μL of luciferin (10 μg/μL; Pierce), and tumor development was monitored using IVIS® System (Perkin Elmer). When the tumor intensity reached ~ 5 to 10×10^8 p/s/cm^2/sr, the animals were used to detect tumor distribution. Mice (n = 4) were i.v. injected with PBS or nanoformulations (containing ~ 1 mg/kg MEL; ~ 0.05 % DiR, w/w). Twelve hours after i.v. injection, tumor distribution was analyzed using IVIS® System (748 nm/780 nm).

2.6. *In vivo* anti-HCC effects of nanoformulation

In addition, when tumor intensity reached ~ 5 to 10×10^8 p/s/cm^2/sr, animals (n = 5) were i.v. treated with PBS or nanoformulations (containing ~ 1 mg/kg MEL) on Day 9, 12 and 15. Tumor growth and animal survival were recorded. In addition, tumors were collected on Day 16 for western blotting experiment as previously described (Guo et al., 2021). Briefly, tumors were homogenized and lysed using ProteinExt® Mammalian Total Protein Extraction Kit (TransGen Biotech, China), and the concentration of proteins was quantified using the BCA Kit (Beyotime Biotech). Subsequently, ~ 35 to 45 μg of proteins were loaded to the SDS-polyacrylamide gel and

electrophoresed at 100 V for 1-1.5 h. Proteins were then transferred onto a polyvinylidene fluoride membrane (Invitrogen) at 200 mA for 1-1.5 h. The membrane was incubated overnight with the primary antibodies (Table S1) at 4℃. The secondary antibody (Table S1) was added to the membrane for 1.5 h, and the proteins were detected using the enhanced chemiluminescence solution (YEASEN Biotech) and quantified using ImageJ.

2.7. Statistical analysis

Results were presented as mean ± standard deviation. The significance of differences was evaluated using one-way ANOVA (Bonferroni's Post-Hoctest) (GraphPad prism). The analysis of body weight, tumor growth and animal survival was evaluated using two-way ANOVA (Bonferroni's Post-Hoctest) (GraphPad prism). In all experiments, $p < 0.05$ was considered statistically significant.

3. Results and Discussion

3.1. Preparation and physicochemical characterization of CD.MEL.PEG-FA

As is a metalloid element with two oxidation states namely As (III) and As (V), and can form organic and inorganic arsenicals. Arsenicals have been historically used as therapeutic agents for different diseases (e.g., dermatosis, hematological malignancies and solid tumors) (Liu et al., 2021). For example, arsenic trioxide (As_2O_3, an inorganic arsenical) has become the established component of first-line treatment protocols for acute promyelocytic leukemia (one of the hematological malignancies) (Yilmaz et al., 2021). In addition, MEL is an organic arsenical, and has been exclusively applied for treating late-stage human African trypanosomiasis (a malignancy caused by protozoan parasites) (Fairlamb and Horn, 2018). MEL is capable of penetrating the BBB to kill parasites inside the CSF (Fairlamb and Horn, 2018). Due to the capacity of

As compounds for apoptotic induction (Liu et al., 2021), the potential of MEL for HCC therapy was assessed in this study. As shown in Fig. S1, MEL caused ~ 50% cell death (IC_{50}) in Hepa1-6 cells at ~ 24 μmol/L, confirming the *in vitro* anti-HCC potential of MEL.

In the clinic, MEL is dissolved in propylene glycol and administered to patients *via* i.v. infusions. However, i.v. administration is painful as propylene glycol is highly irritating to tissues. In addition, i.v. administration of MEL induces non-specific tissue delivery, causing severe toxic effects and even death (Fairlamb and Horn, 2018). Recently, Kennedy et al. have developed two CD derivatives (RAME-CD and HP-CD) to improve solubility and bioavailability of MEL (Gibaud et al., 2005). Following oral administration, the resultant MEL-containing microcomplexes were mainly delivered into the brain, in which they provided therapeutic efficacy against the trypanosome infection in mice, demonstrating the potential for treating human African trypanosomiasis (Rodgers et al., 2011). However, systemic administration of these microcomplexes may not be suitable for HCC therapy in that they are mainly found in the brain, and lack the targeting ligand for facilitating MEL delivery to HCC cells (Ben Zirar et al., 2008) (Rodgers et al., 2011).

Recent advances in nanotechnology and drug formulation expedite the design and application of nano drug delivery systems (NDDS) for chemotherapeutic drugs in cancer therapy (Guo and Huang, 2020) (Sun et al., 2021) (Shan et al., 2022) (Guo and Huang, 2022) (Guo et al., 2023). Thus, developments of emerging NDDS may potentially improve the safety and efficacy of MEL in the treatment of HCC. In order to facilitate *in vivo* anti-HCC potential of MEL, a NDDS was developed in this study by loading MEL into the amphiphilic CD modified with PEGylated FA that could specifically bind to FR on HCC cells (Fig. 1). It has been reported by our laboratories

that the CD could self-assemble into NPs for encapsulating chemotherapeutic drugs, whereby chemotherapeutic drugs were loaded within the hydrophobic cavity and domain of the CD (Zou et al., 2021) (Sun et al., 2022). In this study, HPLC results demonstrated that MEL could be encapsulated within the CD at various weight ratios (WR) of CD and MEL (results not shown), and the optimal EE% (~ 85 wt%) and LC% (~ 14 wt%) of MEL were achieved by the CD at WR5 (Fig. 2A).

Subsequently, the "postinsertion" technique that allows the incorporation of DSPE-PEG-targeting ligands into the preformed liposomes and liposome-like nanostructures (Evans et al., 2017) (Swart et al., 2022), was used to achieve the incorporation of DSPE-PEG and DSPE-PEG-FA onto the CD.MEL nanocomplex (Fig. 1). HPLC results demonstrated that CD.MEL.PEG and CD.MEL.PEG-FA achieved similar EE% (~ 88 and 88 wt%) and LC% (~ 11 and 11 wt%) as compared to CD.MEL (Fig. 2A), indicating that the encapsulation of MEL within CD remained unaffected by the modification of DSPE-PEG and DSPE-PEG-FA. In addition, CD.MEL.PEG and CD.MEL.PEG-FA displayed a significantly higher particle sizes (~ 108 and 110 nm) and reduced surface charge (~ 8 and 9 mV) as compared to CD.MEL (~ 95 nm and 40 mV), suggesting the successful incorporation of DSPE-PEG and DSPE-PEG-FA which masks the surface charge (Fig. 2A). The polydispersity index (PDI) of CD.MEL, CD.MEL.PEG and CD.MEL.PEG-FA was ~ 0.22, 0.31 and 0.32 respectively (Fig. 2A), indicating the generation of monodisperse nanoformulations. Indeed, CD.MEL.PEG-FA displayed a uniform spherical morphology (Fig. 2B), which was similar to the morphologies observed by CD.MEL and CD.MEL.PEG (data not shown).

The release efficiency of MEL from the targeted nanoformulation was assessed under neutral and acidic environments. As shown in Fig. 2C, ~ 10% of MEL were released after 1 h incubation in neutral environment (pH = 7.4), whereas the drug

276 release was significantly ($p < 0.01$) increased (~ 30%) after 1 h incubation in acidic
277 environment (pH = 5.5). After 24 h incubation, ~ 50% and 90% of MEL were released
278 in neutral (pH = 7.4) and acidic (pH = 5.5) environments, respectively. These results
279 show that the targeted nanoformulation achieved significantly higher drug release at
280 acidic pH, which was similar to different amine-modified nanoformulations that were
281 developed by other research groups (Gao et al., 2010) (He et al., 2017) (Zhuo et al.,
282 2020). The mechanism underlying the pH-sensitive drug release of our targeted
283 nanoformulation and others is due to the protonation of the amine groups in response
284 to the acidic environments (Gao et al., 2010) (He et al., 2017) (Zhuo et al., 2020). In
285 addition, following storage at 4 °C, the particle size of the targeted nanoformulation in
286 water remained unchanged (~ 110 to 110 nm) for two weeks (Fig. 2D). The non-targeted
287 nanoformulation also achieved similar drug release and stability to those recorded by
288 FA-targeted counterpart. However, the aggregation was detected with the CD.MEL
289 nanocomplex during the drug release and stability experiments. These results indicate
290 that the PEG incorporation efficiently masked the surface of the CD.MEL nanocomplex
291 to improve the particle stability. Due to the instability, CD.MEL was not used in the
292 following *in vitro* and *in vivo* experiments.

293 **3.2. *In vitro* anti-HCC effects of CD.MEL.PEG-FA**

294 The *in vitro* anti-HCC property of the targeted nanoformulation (CD.MEL.PEG-
295 FA) was first studied using the MTT assay in Hepa1-6 cells, which is a mouse HCC
296 cell line that has been widely used to determine the targeted delivery efficacy of FA-
297 modified nanoformulations (Hu et al., 2017) (Maghsoudinia et al., 2021a)
298 (Maghsoudinia et al., 2021b) (Gong et al., 2021). As shown in Fig. S1, MEL on its own
299 achieved an IC_{50} at ~ 24 μmol/L (24 h incubation), while the cytotoxicity was
300 significantly increased ($p < 0.05$) by CD.MEL.PEG-FA ($IC_{50} \approx 15$ μg/mL of MEL) (Fig.

S1). The anti-HCC activity mainly resulted from cell-specific delivery of MEL *via* the FA-FR-associated pathway, as NPs without MEL caused no cell death (Fig. S1). Indeed, CD.MEL.PEG-FA at the same concentrations of MEL also induced significantly ($p < 0.05$) higher cytotoxicity as compared to CD.MEL.PEG (Fig. 3A), confirming the function of FA as a targeting ligand for HCC-specific drug delivery.

To further confirm the active targeting delivery, the cellular uptake of CD.MEL.PEG and CD.MEL.PEG-FA containing rhodamine was investigated using confocal microscopy. As shown in Fig. 3B, the cellular uptake achieved by the targeted nanoformulation containing rhodamine was significantly (the relative fluorescence intensity ≈ 38% after 8 h incubation; $p < 0.05$) higher than PBS (0%) and the non-targeted counterpart (~ 20%) (Fig. 3B), further confirming the role of the FA targeting ligand in facilitating HCC-specific drug delivery.

In addition, the targeted nanoformulation caused significantly higher HCC cell apoptosis (~ 50% after 24 h incubation; $p < 0.01$) as compared to PBS (< 1%) and the non-targeted counterpart (~ 20%) (Fig. 3C). Moreover, the targeted nanoformulation significantly inhibited HCC cell migration (the cell-free area after treatment *vs.* the cell-free area before treatment > 90% after 24 h incubation; $p < 0.01$) as compared to PBS (~ 40%) and non-targeted counterpart (~ 50%) (Fig. 3D). Therefore, results in Fig. 3 indicate that MEL-mediated apoptosis is the main mechanism for CD.MEL.PEG-FA to suppress the HCC cell growth and migration.

3.3. *In vivo* toxicity and tumor distribution of CD.MEL.PEG-FA

The *in vivo* toxicity of the targeted nanoformulation was evaluated in the healthy mice (n = 4). It is known that the i.v. administration of MEL is painful and causes severe tissue damage (Fairlamb and Horn, 2018). Indeed, toxic signs (e.g., body weight loss, hunched posture and ruffled hair coat) were observed in mice following i.v. injections

of MEL at a dose of 1 mg/kg (Fig. S2). In contrast, no body weight loss was observed in mice i.v. administrated with CD.MEL.PEG-FA relative to PBS (Fig. 4A). In addition, results of H&E staining experiments demonstrated that no histopathology was found in the heart, liver, spleen, lung and kidneys of mice after i.v. injections of CD.MEL.PEG-FA as compared to PBS (Fig. 4B). Moreover, no alteration in alanine aminotransferase (ALT), aspartate aminotransferase (AST), urea nitrogen (BUN) and creatinine (CRE) was detected, indicating that no hepatic and renal injury was caused by CD.MEL.PEG-FA when compared with PBS (Fig. 4C). These results show that no systemic toxicity was caused by the targeted nanoformulation under the conditions tested.

To confirm tumor targeting delivery, the tumor distribution of CD.MEL.PEG-FA was determined in Hepa1-6-Luc-derived orthotopic HCC mice. Results show that CD.MEL.PEG-FA was significantly ($p < 0.05$) located in the liver tumor area as compared to CD.MEL.PEG, and this was confirmed by the overlapping of NP (DiR dye) and the tumor (luciferase in tumor cells) (Fig. 4D). These results indicate that the targeted nanoformulation, due to targeting the FR expressed on HCC cells, can promote tumor targeting delivery.

3.4. *In vivo* anti-HCC effects of CD.MEL.PEG-FA

Subsequently, the therapeutic efficacy of the targeted nanoformulation was assessed using Hepa1-6-Luc-derived orthotopic HCC mice (n = 5). Due to the fact that free MEL caused toxic signs (Fig. S2), animals were i.v. treated with PBS, CD.MEL.PEG, and CD.MEL.PEG-FA (Fig. 5A). As shown in Fig. 5B, CD.MEL.PEG significantly ($p < 0.05$) suppressed tumor growth as compared to PBS, while tumor growth was further ($p < 0.01$) retarded by CD.MEL.PEG-FA relative to PBS and CD.MEL.PEG. As a result, CD.MEL.PEG-FA significantly ($p < 0.01$) prolonged the survival of diseased animals relative to PBS and CD.MEL.PEG (Fig. 5C). In addition,

CD.MEL.PEG-FA caused significantly higher apoptosis ($p < 0.05$) in tumor cells than PBS and CD.MEL.PEG, which was confirmed by the increased expression of Bax and cleaved-Caspase 3 proteins (two key apoptosis-triggering proteins) and the reduced expression of Bcl-2 protein (a key apoptosis-inhibitory protein) (Fig. 5D). Thus, results in Fig. 5 indicate that the anti-HCC efficacy of the targeted nanoformulation resulted mainly from tumor-specific delivery of MEL and from MEL-mediated apoptosis.

Recent developments of emerging NDDS effectively promote anticancer efficacy and alleviate toxic effects of arsenic and its compounds (Fei et al., 2020) (Fu et al., 2020). Since As_2O_3 has become the pioneer arsenic-containing drug, the design and formulation of As_2O_3 NDDS have attracted more attention in the fields of drug delivery and cancer therapy (Sonksen et al., 2022). However, NDDS for MEL delivery have been much less studied. One example includes that MEL-containing nanosuspensions were prepared using Pluronic F-68® (poloxamer 188) or Pluronic F-127® (poloxamer 407) and mannitol (Ben Zirar et al., 2008). However, these nanosuspensions have not been applied for HCC therapy as they do not have the HCC-targeting ligand and may not specifically deliver MEL to the tumors (Ben Zirar et al., 2008). Consequently, the FA-targeted PEGylated amphiphilic CD NP developed in this study is to our knowledge the first nano delivery system to achieve safe, efficient and specific delivery of MEL against HCC (Fig. 4 and 5).

4. Conclusions

In this study, an amphiphilic CD was used to develop a FA-targeted PEGylated nano delivery vector for formulating MEL (Fig. 1). The resultant NDDS (CD.MEL.PEG-FA) demonstrated favorable physicochemical properties, in terms of drug loading (EE% ≈ 88 wt% and LC% ≈ 11 wt%), particle size (~ 110 nm), zeta

potential (~ 9 mV), pH-sensitive drug release (higher MEL release in acidic condition), and storage stability (no aggregation for two weeks) (Fig. 2). These physicochemical properties were compliant with the requirements for favorable *in vitro and in vivo* delivery fates (Fig. 3 and 4). Indeed, the tumor growth was significantly retarded following i.v. administration of CD.MEL.PEG-FA (Fig. 5), indicating the HCC-specific delivery of MEL, without inducing obvious toxic signs. Our study demonstrates great potential of CD.MEL.PEG-FA as an emerging chemotherapy option for treating HCC.

Acknowledgments

This work was supported by the National Natural Science Foundation of China (81770026), the Science and Technology Department of Jilin Province (YDZJ202201ZYTS528), the Cross Discipline Project of First Hospital of Jilin University, China (JDYYJCHX2020001), the Norman Bethune Program of Jilin University, China (2022B40), the "Medicine + X" Interdisciplinary Innovation Team of Norman Bethune Health Science Center of Jilin University, China (2022JBGS05), and the Science Foundation Ireland co-funded under the European Regional Development: Centre for Research in Medical Devices, CURAM (13/RC/2073, Ireland), Synthesis and Solid State Cluster, SSPC (12/RC/2275, Ireland), and Centre for Advanced Materials and BioEngineering Research, AMBER (12/RC/2275, Ireland).

Conflicts of interest

Authors declares no conflict of interest.

Figure legends

Figure 1. The formulation schematic of CD.MEL.PEG-FA.

Figure 2. Physicochemical characterization of CD.MEL.PEG-FA. (A) The EE%, LC%, particle size, surface charge and PDI of nanoformulations (n = 4). (B) TEM image of FA-targeted nanoformulation (scale bar = 100 nm). (C) The release of MEL from FA-targeted nanoformulation in 0.01 M PBS (pH = 5.5 and 7.4) at 37 ^{o}C (n = 5, * $p < 0.05$). (D) The particle size of FA-targeted nanoformulation in aqueous solution stored at 4 ^{o}C (n = 5, * $p < 0.05$, ** $p < 0.01$ and NS = no significance).

Figure 3. *In vitro* characterization of CD.MEL.PEG-FA in Hepa1-6 cells. (A) Cell viability after 24 h treatment of CD.MEL.PEG and CD.MEL.PEG-FA at different concentrations (n = 4, * $p < 0.05$ and NS = no significance). (B) The cellular uptake after 8 h incubation of CD.MEL.PEG and CD.MEL.PEG-FA (5 μmol/L MEL; 0.05 % rhodamine, w/w) (n = 3, * $p < 0.05$ and ** $p < 0.01$) (scale bar = 10 μm). (C) Apoptotic cells (%) after 24 h treatment of CD.MEL.PEG and CD.MEL.PEG-FA (15 μmol/L MEL) (n = 4, * $p < 0.05$ and ** $p < 0.01$). (D) Relative scratch area (%) before and after 24 h treatment of CD.MEL.PEG and CD.MEL.PEG-FA (15 μmol/L MEL) (n = 4, * $p < 0.05$ and NS = no significance).

Figure 4. *In vivo* toxicity and tumor distribution of CD.MEL.PEG-FA. (A) The body weight of healthy C57BL/6 mice over a 25-day period after i.v. injections of PBS and CD.MEL.PEG-FA (1 mg/kg MEL) on Day 1, 5, 9, 12 and 17 (n = 4). (B) The heart, liver, spleen, lung and kidneys were collected on Day 25 and assessed using H&E staining assay (scale bar = 100 μm). (C) The liver/kidney functions (alanine aminotransferase (ALT), aspartate aminotransferase (AST), blood urea nitrogen (BUN) and creatinine (CRE)) on Day 25 (n = 4). (D) Tumor distribution of DiR-labeled nanoformulations at 12 h following i.v. injection in Hepa1-6-Luc derived orthotopic HCC mice.

Figure 5. *In vivo* anti-HCC activity of CD.MEL.PEG-FA in Hepa1-6-Luc derived

orthotopic HCC mice. (A) HCC development and treatment schedule (red arrow = i.v. injection). (B) The tumor growth following the treatment of PBS, CD.MEL.PEG and CD.MEL.PEG-FA (1 mg/kg MEL) over a 35-day period following the treatment schedule as shown in Fig. 5 A (n = 5, * $p < 0.05$). (C) Animal survival (median survival: PBS for ~ 26 days, CD.MEL.PEG for ~ 42 days, and CD.MEL.PEG-FA for ~ 64 days) (n = 5, * $p < 0.05$). (D) The protein expression in the Bax/Bcl-2/caspase 3 signaling cascade within the tumors one day (Day 16) following the treatment schedule as shown in Fig. 5 A (n = 4, * $p < 0.05$ and ** $p < 0.01$).

References

Ben Zirar, S., Astier, A., Muchow, M., Gibaud, S., 2008. Comparison of nanosuspensions and hydroxypropyl-beta-cyclodextrin complex of melarsoprol: pharmacokinetics and tissue distribution in mice. Eur J Pharm Biopharm 70, 649-656.

Evans, J.C., Malhotra, M., Fitzgerald, K.A., Guo, J., Cronin, M.F., Curtin, C.M., O'Brien, F.J., Darcy, R., O'Driscoll, C.M., 2017. Formulation and Evaluation of Anisamide-Targeted Amphiphilic Cyclodextrin Nanoparticles To Promote Therapeutic Gene Silencing in a 3D Prostate Cancer Bone Metastases Model. Mol Pharm 14, 42-52.

Fairlamb, A.H., Horn, D., 2018. Melarsoprol Resistance in African Trypanosomiasis. Trends Parasitol 34, 481-492.

Fei, W., Li, C., Tao, J., Cai, X., Yao, W., Ye, Y., Zhang, Y., Yao, Y., Song, Q., Li, F., Zheng, C., 2020. Construction of arsenic-metal complexes loaded nanodrugs for solid tumor therapy: A mini review. Int J Pharm 583, 119385.

Fu, X., Li, Y.S., Zhao, J., Yu, L.L., Luo, R.G., Liang, Q.R., Tang, Q., 2020. Will Arsenic Trioxide Benefit Treatment of Solid Tumor by Nano- Encapsulation? Mini Rev Med Chem 20, 239-251.

Galle, P.R., Dufour, J.F., Peck-Radosavljevic, M., Trojan, J., Vogel, A., 2021. Systemic therapy of advanced hepatocellular carcinoma. Future Oncol 17, 1237-1251.

Gao, W., Chan, J.M., Farokhzad, O.C., 2010. pH-Responsive nanoparticles for drug delivery. Mol Pharm 7, 1913-1920.

Gibaud, S., Zirar, S.B., Mutzenhardt, P., Fries, I., Astier, A., 2005. Melarsoprol-cyclodextrins inclusion complexes. Int J Pharm 306, 107-121.

Gong, T., Wang, X., Ma, Q., Li, J., Li, M., Huang, Y., Liang, W., Su, D., Guo, R., 2021. Triformyl cholic acid and folic acid functionalized magnetic graphene oxide nanocomposites: Multiple-targeted dual-modal synergistic chemotherapy/photothermal therapy for liver cancer. J Inorg Biochem 223, 111558.

Guo, J., Huang, L., 2020. Membrane-core nanoparticles for cancer nanomedicine. Adv Drug Deliv Rev 156, 23-39.

Guo, J., Huang, L., 2022. Nanodelivery of cGAS-STING activators for tumor immunotherapy. Trends Pharmacol Sci 43, 957-972.

Guo, J., Ogier, J.R., Desgranges, S., Darcy, R., O'Driscoll, C., 2012. Anisamide-targeted cyclodextrin nanoparticles for siRNA delivery to prostate tumours in mice. Biomaterials 33, 7775-7784.

Guo, J., Yu, Z., Das, M., Huang, L., 2020. Nano Codelivery of Oxaliplatin and Folinic Acid Achieves Synergistic Chemo-Immunotherapy with 5-Fluorouracil for Colorectal Cancer and Liver Metastasis. ACS Nano 14, 5075-5089.

Guo, J., Yu, Z., Sun, D., Zou, Y., Liu, Y., Huang, L., 2021. Two nanoformulations induce reactive oxygen species and immunogenetic cell death for synergistic chemo-immunotherapy eradicating colorectal cancer and hepatocellular carcinoma. Mol Cancer 20, 10.

Guo, J., Zou, Y., Huang, L., 2023. Nano Delivery of Chemotherapeutic ICD Inducers for Tumor Immunotherapy. Small Methods, e2201307.

Han, S., Bi, S., Guo, T., Sun, D., Zou, Y., Wang, L., Song, L., Chu, D., Liao, A., Song, X., Yu, Z., Guo, J., 2022. Nano co-delivery of Plumbagin and Dihydrotanshinone I reverses immunosuppressive TME of liver cancer. J Control Release 348, 250-263.

He, Y., Luo, L., Liang, S., Long, M., Xu, H., 2017. Amino-functionalized mesoporous silica nanoparticles as efficient carriers for anticancer drug delivery. J Biomater Appl 32, 524-532.

Hu, Z., Chen, J., Zhou, S., Yang, N., Duan, S., Zhang, Z., Su, J., He, J., Zhang, Z., Lu, X., Zhao, Y., 2017. Mouse IP-10 Gene Delivered by Folate-modified Chitosan Nanoparticles and Dendritic/tumor Cells Fusion Vaccine Effectively Inhibit the Growth of Hepatocellular Carcinoma in Mice. Theranostics 7, 1942-1952.

Kennedy, P.G., 2006. Human African trypanosomiasis-neurological aspects. J Neurol 253, 411-416.

Koirala, N., Das, D., Fayazzadeh, E., Sen, S., McClain, A., Puskas, J.E., Drazba, J.A., McLennan, G., 2019. Folic acid conjugated polymeric drug delivery vehicle for targeted cancer detection in hepatocellular carcinoma. J Biomed Mater Res A 107, 2522-2535.

Liu, G., Song, Y., Li, C., Liu, R., Chen, Y., Yu, L., Huang, Q., Zhu, D., Lu, C., Yu, X., Xiao, C., Liu, Y., 2021. Arsenic compounds: The wide application and mechanisms applied in acute promyelocytic leukemia and carcinogenic toxicology. Eur J Med Chem 221, 113519.

Llovet, J.M., Montal, R., Sia, D., Finn, R.S., 2018. Molecular therapies and precision medicine for hepatocellular carcinoma. Nat Rev Clin Oncol 15, 599-616.

Luan, X., Rahme, K., Cong, Z., Wang, L., Zou, Y., He, Y., Yang, H., Holmes, J.D., O'Driscoll, C.M., Guo, J., 2019. Anisamide-targeted PEGylated gold nanoparticles designed to target prostate cancer mediate: Enhanced systemic exposure of siRNA, tumour growth suppression and a synergistic therapeutic response in combination with paclitaxel in mice. Eur J Pharm Biopharm 137, 56-67.

505 Maghsoudinia, F., Tavakoli, M.B., Samani, R.K., Hejazi, S.H., Sobhani, T., Mehradnia,
506 F., Mehrgardi, M.A., 2021a. Folic acid-functionalized gadolinium-loaded phase
507 transition nanodroplets for dual-modal ultrasound/magnetic resonance imaging of
508 hepatocellular carcinoma. Talanta 228, 122245.
509 Maghsoudinia, F., Tavakoli, M.B., Samani, R.K., Motaghi, H., Hejazi, S.H., Mehrgardi,
510 M.A., 2021b. Bevacizumab and folic acid dual-targeted gadolinium-carbon dots for
511 fluorescence/magnetic resonance imaging of hepatocellular carcinoma. Journal of Drug
512 Delivery Science and Technology 61, 102288.
513 O'Mahony, A.M., Ogier, J., Desgranges, S., Cryan, J.F., Darcy, R., O'Driscoll, C.M.,
514 2012. A click chemistry route to 2-functionalised PEGylated and cationic beta-
515 cyclodextrins: co-formulation opportunities for siRNA delivery. Org Biomol Chem 10,
516 4954-4960.
517 Rodgers, J., Jones, A., Gibaud, S., Bradley, B., McCabe, C., Barrett, M.P., Gettinby, G.,
518 Kennedy, P.G., 2011. Melarsoprol cyclodextrin inclusion complexes as promising oral
519 candidates for the treatment of human African trypanosomiasis. PLoS Negl Trop Dis 5,
520 e1308.
521 Shan, X., Gong, X., Li, J., Wen, J., Li, Y., Zhang, Z., 2022. Current approaches of
522 nanomedicines in the market and various stage of clinical translation. Acta Pharm Sin
523 B 12, 3028-3048.
524 Sonksen, M., Kerl, K., Bunzen, H., 2022. Current status and future prospects of
525 nanomedicine for arsenic trioxide delivery to solid tumors. Med Res Rev 42, 374-398.
526 Sun, D., Zhang, J., Wang, L., Yu, Z., O'Driscoll, C.M., Guo, J., 2021. Nanodelivery of
527 immunogenic cell death-inducers for cancer immunotherapy. Drug Discov Today 26,
528 651-662.
529 Sun, D., Zou, Y., Song, L., Han, S., Yang, H., Chu, D., Dai, Y., Ma, J., O'Driscoll, C.M.,
530 Yu, Z., Guo, J., 2022. A cyclodextrin-based nanoformulation achieves co-delivery of
531 ginsenoside Rg3 and quercetin for chemo-immunotherapy in colorectal cancer. Acta
532 Pharm Sin B 12, 378-393.

Sung, H., Ferlay, J., Siegel, R.L., Laversanne, M., Soerjomataram, I., Jemal, A., Bray, F., 2021. Global Cancer Statistics 2020: GLOBOCAN Estimates of Incidence and Mortality Worldwide for 36 Cancers in 185 Countries. CA Cancer J Clin 71, 209-249.

Swart, L.E., Koekman, C.A., Seinen, C.W., Issa, H., Rasouli, M., Schiffelers, R.M., Heidenreich, O., 2022. A robust post-insertion method for the preparation of targeted siRNA LNPs. Int J Pharm 620, 121741.

Yang, H., Song, L., Sun, B., Chu, D., Yang, L., Li, M., Li, H., Dai, Y., Yu, Z., Guo, J., 2021. Modulation of macrophages by a paeoniflorin-loaded hyaluronic acid-based hydrogel promotes diabetic wound healing. Mater Today Bio 12, 100139.

Yilmaz, M., Kantarjian, H., Ravandi, F., 2021. Acute promyelocytic leukemia current treatment algorithms. Blood Cancer J 11, 123.

Yu, Z., Guo, J., Hu, M., Gao, Y., Huang, L., 2020. Icaritin Exacerbates Mitophagy and Synergizes with Doxorubicin to Induce Immunogenic Cell Death in Hepatocellular Carcinoma. ACS Nano 14, 4816-4828.

Zhuo, S., Zhang, F., Yu, J., Zhang, X., Yang, G., Liu, X., 2020. pH-Sensitive Biomaterials for Drug Delivery. Molecules 25, 5649.

Zou, Y., Xiao, F., Song, L., Sun, B., Sun, D., Chu, D., Wang, L., Han, S., Yu, Z., O'Driscoll, C.M., Guo, J., 2021. A folate-targeted PEGylated cyclodextrin-based nanoformulation achieves co-delivery of docetaxel and siRNA for colorectal cancer. Int J Pharm 606, 120888.

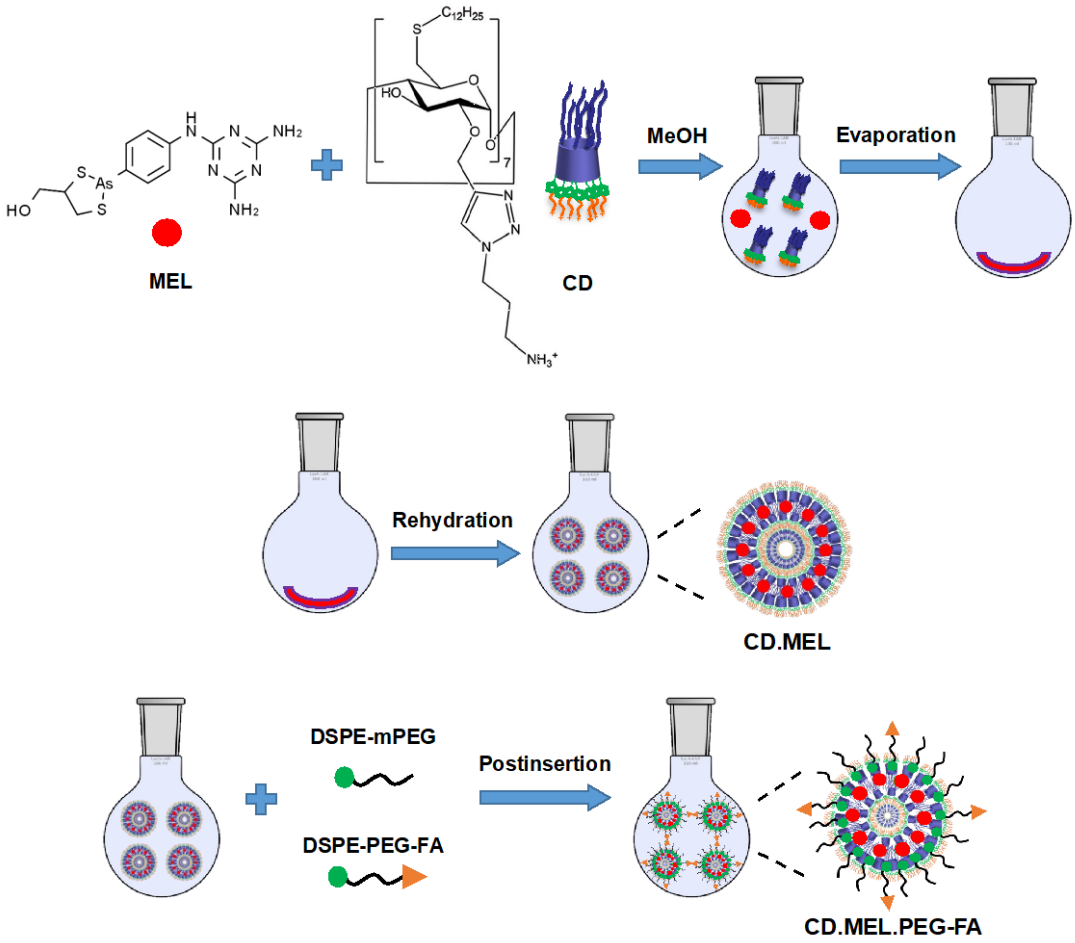
MEL
CD
MeOH
Evaporation
Rehydration
CD.MEL
DSPE-mPEG
DSPE-PEG-FA
Postinsertion
CD.MEL.PEG-FA

Figure 1.

A

Nanoformulation	WR	EE%	LC%	Size (nm)	Charge (mV)	PDI
CD.MEL	5:1	85 ± 2	14 ± 3	95 ± 5 nm	40 ± 5 mV	0.22
CD.MEL.PEG	5:1:2.5	88 ± 4	11 ± 3	108 ± 3 nm	8 ± 3 mV	0.31
CD.MEL.PEG-FA	5:1:2.5	88 ± 3	11 ± 2	110 ± 2 nm	9 ± 3 mV	0.32

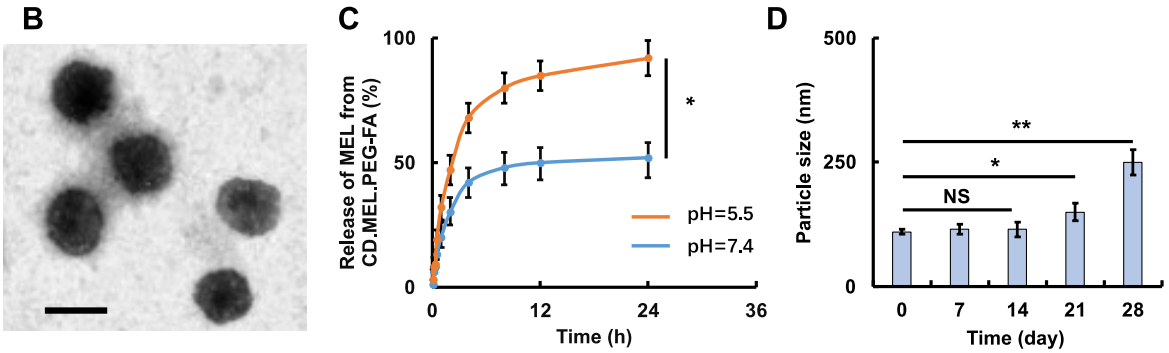

Figure 2.

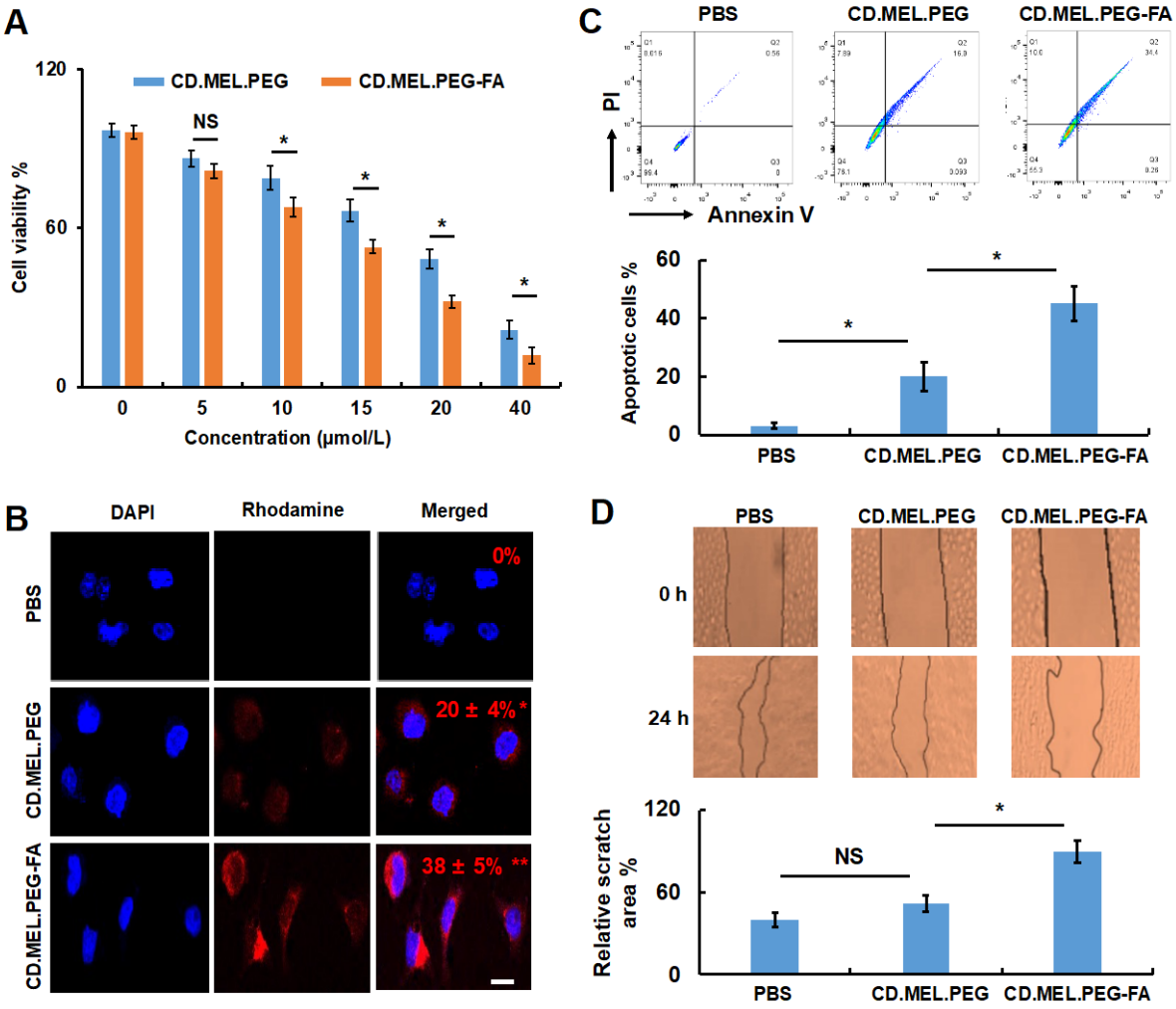
A
120
60
0
Cell viability %
CD.MEL.PEG
CD.MEL.PEG-FA
NS
*
0
5
10
15
20
40
Concentration (μmol/L)
B
DAPI
Rhodamine
Merged
PBS
CD.MEL.PEG
CD.MEL.PEG-FA
0%
20 ± 4% *
38 ± 5% **
C
PBS
CD.MEL.PEG
CD.MEL.PEG-FA
PI
Annexin V
Apoptotic cells %
60
40
20
0
D
0 h
24 h
Relative scratch area %
120
60
0
NS

Figure 3.

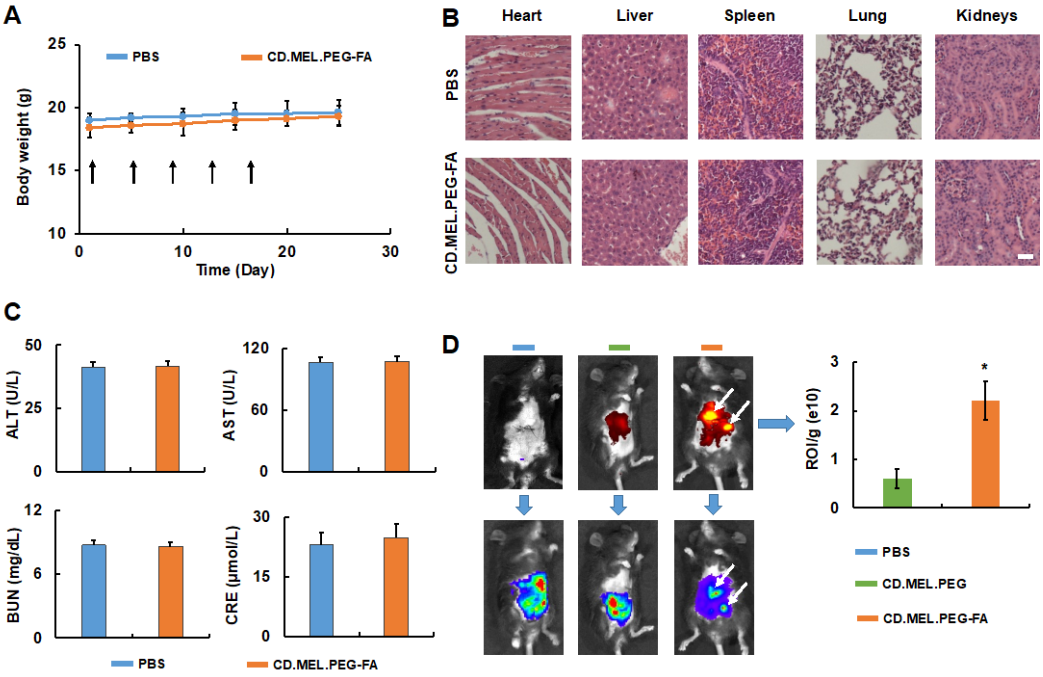
A
PBS
CD.MEL.PEG-FA
Body weight (g)
Time (Day)
B
Heart
Liver
Spleen
Lung
Kidneys
PBS
CD.MEL.PEG-FA
C
ALT (U/L)
AST (U/L)
BUN (mg/dL)
CRE (μmol/L)
PBS
CD.MEL.PEG-FA
D
ROI/g (e10)
PBS
CD.MEL.PEG
CD.MEL.PEG-FA

Figure 4.

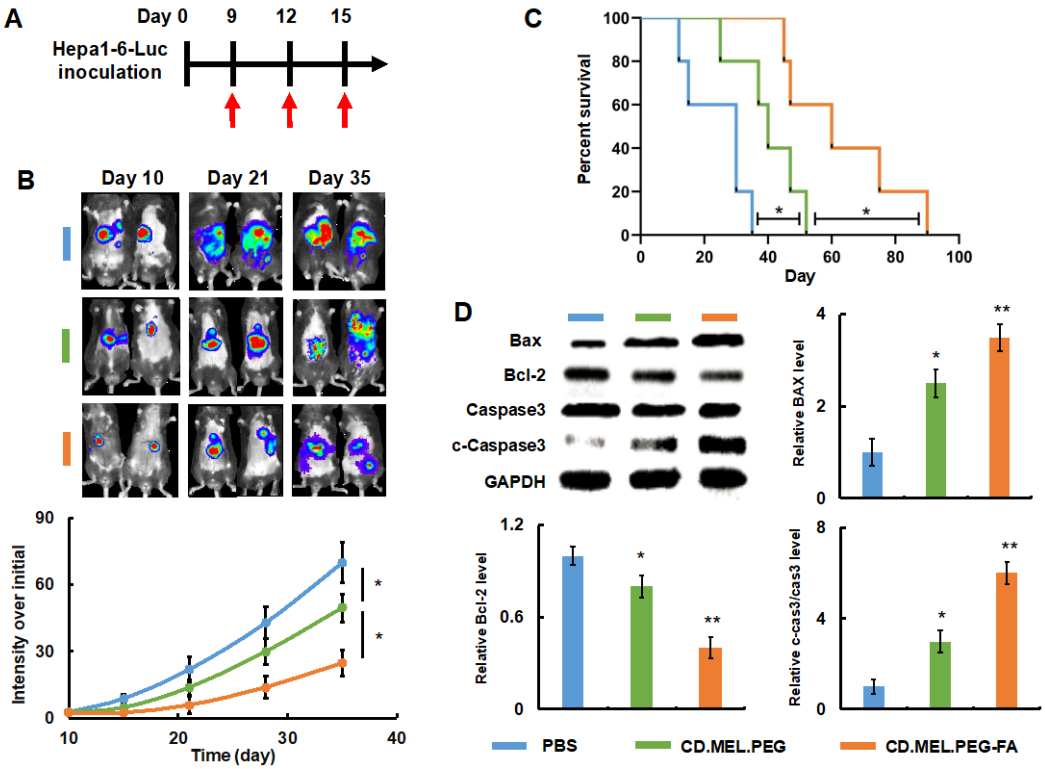
A
Day 0
9
12
15
Hepa1-6-Luc inoculation
B
Day 10
Day 21
Day 35
Intensity over initial
Time (day)
C
Percent survival
Day
D
Bax
Bcl-2
Caspase3
c-Caspase3
GAPDH
Relative BAX level
Relative Bcl-2 level
Relative c-cas3/cas3 level
PBS
CD.MEL.PEG
CD.MEL.PEG-FA

Figure 5.